JACS
JOURNAL OF THE AMERICAN CHEMICAL SOCIETY
Communication
pubs.acs.org/JACS

Colloidal Synthesis of Magnetic $CuCr_2S_4$ Nanocrystals and Nanoclusters

Karthik Ramasamy, Dipanjan Mazumdar, Ziyou Zhou, Yu-Hsiang A. Wang, and Arunava Gupta*

Center for Materials for Information Technology, The University of Alabama, Tuscaloosa, Alabama 35487, United States

Supporting Information

ABSTRACT: Nanocrystals and nanoclusters of the room-temperature magnetic spinel $CuCr_2S_4$ have been synthesized using a facile solution-based method. The synthesis involves hot injection of an excess of 1-dodecanethiol (1-DDT) into a boiling coordinating solvent containing $CuCl_2$ and $CrCl_3{\cdot}6H_2O$. Using octadecylamine (ODA) as a solvent yields cube-shaped nanocrystals with an average size of 20 ± 2 nm, while with oleylamine (OLA), nanoclusters with an average size of 31 ± 2.5 nm are obtained. In both cases, powder X-ray diffraction patterns confirmed the formation of the pure spinel phase without any impurities. While the synthesized powders are superparamagnetic near room temperature, they exhibit ferromagnetic behavior at lower temperatures, with magnetization (M_S) values of 30 emu/g (1.63 μ_B/f.u.) and 33 emu/g (1.79 μ_B/f.u.) for the ODA- and OLA-capped nanocrystals and nanoclusters, respectively, at 5 K.

Magnetic materials with critical dimensions on the order of nanometer scale display unique properties such as superparamagnetism, high field irreversibility, and high saturation field due to surface anisotropy contributions.[1] Such materials have broad applicability, including in magnetic recording media, magnetic seals, and biomedical applications.[2] Tailoring of the nanomaterial properties and applications is primarily dictated by their size and shape, which can often be controlled by the synthetic methodology.[3] The established synthetic methodologies for magnetic nanomaterials (transition metals, metal alloys, and metal oxides) generally involve the thermal decomposition of metallic precursors, the polyol method, electrochemical reduction, and chemical reduction.[4] However, syntheses of a large class of magnetic chromium-based chalcogenide nanoparticles are limited in the literature. This omission can primarily be attributed to the complications involved in the control of the oxidation state of chromium.[5] Chromium-based chalcogenide spinels (chalcospinels), such as $CuCr_2X_4$, $CdCr_2X_4$, $ZnCr_2X_4$, $HgCr_2X_4$, $FeCr_2X_4$, and $CoCr_2X_4$ (X = S, Se, Te), are magnetic metals, semiconductors, or insulators.[6]

Among the chalcospinels, Cu- and Cr-based systems are unique in that they are ferromagnetic at room temperature [with Curie temperatures (T_C) of 377, 430, and 360 K for $CuCr_2S_4$, $CuCr_2Se_4$, $CuCr_2Te_4$, respectively] and are also metallic.[7] In these compounds, Cu and Cr occupy the A and B sites of the normal spinel structure, and the magnetism likely arises from mixed-valence states of chromium [Cr(III) and Cr(IV)].[8] Magneto-optical effects due to the high T_C with metallic characteristics make these materials interesting candidates for study.[9] A number of theoretical studies to help in understanding the origin of magnetism in these materials have been reported.[10] We recently predicted the occurrence of half-metallicity both in cation- and anion-substituted chalcospinels [$Cu(Cd)Cr_2S(Se)_{4-x}$, $CuCr_2S(Se)_{4-x}E_x$ (E = F, Cl, Br), and $CdCr_2S(Se)_{4-x}D_x$ (D = N, P, As)].[11] The use of these materials for spin-transport applications is a growing area of research.[12]

In recent years, there have been a few reports on the solution-based synthesis of $CuCr_2Se_4$ nanoparticles; however, their S and Te analogues are conspicuously absent.[13] Finding a suitable S or Te source and identifying appropriate experimental conditions that would yield the desired spinel phase are the major complications associated with these systems. The selective synthesis of phase-pure chalcospinels without any secondary impurities is challenging. Muroi et al.[14] prepared $CuCr_2S_4$ nanoparticles by mechanical ball milling of stoichiometric amounts of the constituent elements. The milled particles produced a mixture of Cr_2S_3 or Cr_3S_4 with $CuCr_2S_4$, but the morphology and size of the particles was not reported. The formation of impurities has also been observed in conventional ceramic processing.[7,8] Herein we report the first colloidal synthesis of phase-pure $CuCr_2S_4$ nanocrystals and nanoclusters using a solution-based method. The synthesis involves hot injection of excess 1-dodecanethiol (1-DDT) into boiling oleylamine (OLA) or octadecylamine (ODA) solutions containing copper and chromium chlorides.

All of the experiments were carried out in a fume hood under a N_2 atmosphere using standard Schlenk techniques. In a typical synthesis of $CuCr_2S_4$, 0.25 mmol of $CuCl_2$, 0.50 mmol of $CrCl_3{\cdot}6H_2O$, and 10 g of ODA were deaerated at room temperature for 15 min and then back-filled with N_2 for 15 min. The mixture was subsequently heated to 160−165 °C under vacuum and then to 360 °C under N_2. In a separate vessel, 2 mL (3 mmol) of 1-DDT was heated to 245−250 °C under N_2. At 360 °C, 2 mL of the hot 1-DDT was rapidly injected into the metal halide solution, while not permitting the temperature of the solution to decrease below 340 °C. The vessel was then quickly reheated to 360 °C, and the resulting black mixture was continually stirred at this temperature for 1 h. After the mixture was cooled to room temperature, a mixture of hexane (5 mL) and ethanol (15 mL) was added to precipitate the product. The black precipitate was then isolated via centrifugation (7000

Received: October 11, 2011
Published: November 29, 2011

   dx.doi.org/10.1021/ja209575w | J. Am. Chem.Soc. 2011, 133, 20716–20719

rpm). The washing process was repeated three times to ensure removal of any excess capping agent. The desired $CuCr_2S_4$ product was obtained in 70−75% yield. A similar experimental procedure was followed for the synthesis of OLA-capped nanoclusters. A pictorial representation of the synthesis of $CuCr_2S_4$ nanocrystals and nanoclusters is provided in Figure S1 in the Supporting Information.

In the synthesis of $CuCr_2S_4$ nanostructures, we have determined that reaction temperatures below 350 °C predominantly favor the formation of the nonmagnetic secondary phase $CuCrS_2$, as confirmed by powder X-ray diffraction (PXRD) (Figure S2). The use of other conventional shape-directing coordinating solvents (e.g., trioctylphosphine oxide, hexadecylamine, oleic acid, octadecane, etc.) and also the reaction of elemental sulfur with trioctylphosphine or diethyldithiocarbamate complexes of copper and chromium failed to produce the desired spinel phase. This may be due to the high volatility of elemental sulfur or undesired reactions with the solvent at the elevated temperatures, which lead to the formation of secondary phases such as $CuCrS_2$, Cu_xS, Cr_2S_3, or Cr_3S_4.

The phase purity of the synthesized nanocubes and nanoclusters at 360 °C was confirmed by PXRD, which indicated the expected spinel structure (fcc, space group *Fd*3*m*), as shown in Figure 1. The major diffraction peaks are

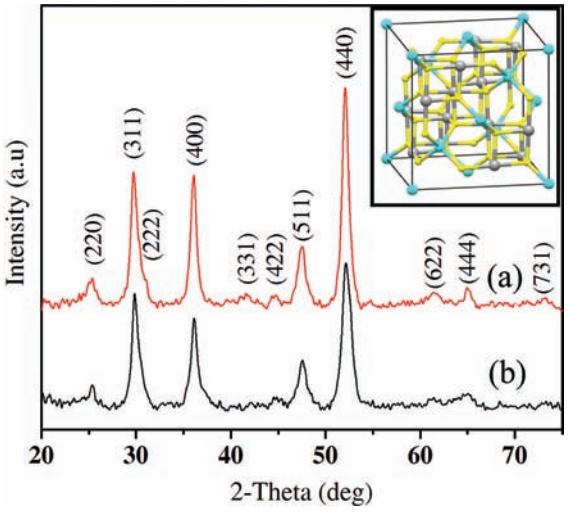

Figure 1. PXRD patterns of (a) nanocubes and (b) nanoclusters. The inset shows the crystal structure of spinel $CuCr_2S_4$ (Cu, blue; Cr, gray; S, yellow).

indexed as (311), (400), (511), (440), (622), and (444) reflections of cubic $CuCr_2S_4$ (ICDD no. 21-0287) with calculated lattice parameters (a) of 9.922 Å and 9.916 for ODA- and OLA-capped particles, respectively (9.814 Å reported for the bulk).[11] The particle size estimated using the Scherrer equation for the (400) reflection peak width was ~18 nm from ODA and ~27 nm from OLA, in good agreement with transmission electron microscopy (TEM) measurements.

We investigated the morphology and structure of the nanocrystals and nanoclusters by TEM. The images in Figure 2 show nearly perfect cubic-shaped particles with size of 20 ± 2 nm (edge-to-edge) prepared in ODA. The size and shape of the nanocrystals are uniform over a large area, as shown in the high-resolution field-emission scanning electron microscopy (FE-SEM) image (Figure S3). High-resolution TEM (HRTEM)

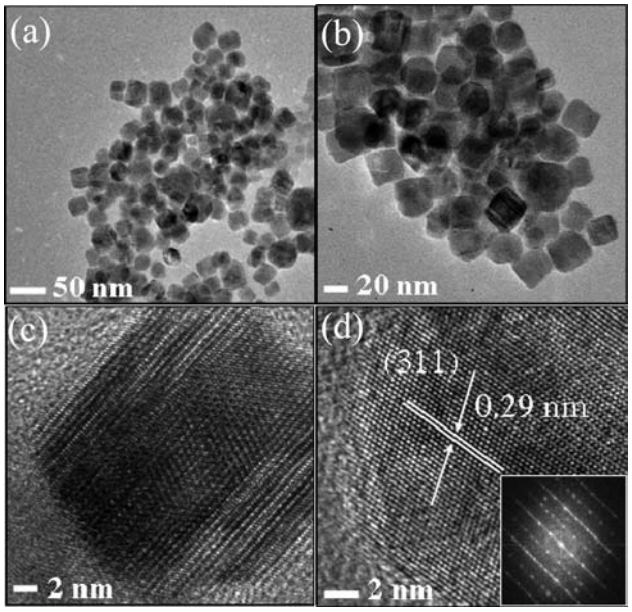

Figure 2. (a, b) TEM images of $CuCr_2S_4$ nanocubes. (c, d) HRTEM images of individual nanocubes. The inset in (d) shows the FFT pattern extracted from the image in (d).

images show lattice fringes with a measured d spacing of 0.29 nm, corresponding to the (311) reflection of spinel $CuCr_2S_4$. The angle between the planes, as measured from the fast Fourier transform (FFT) pattern (Figure 2d inset) obtained from Figure 2d, was determined to be 60°, which is consistent with the expected value for these two planes in a cubic crystal lattice. The FFT pattern shows bright spots with a d spacing of 2.92 Å perpendicular to the lattice fringes, confirming growth along the (311) direction of the cubic phase imaged down the [111] zone axis. The TEM images in Figure 3 show

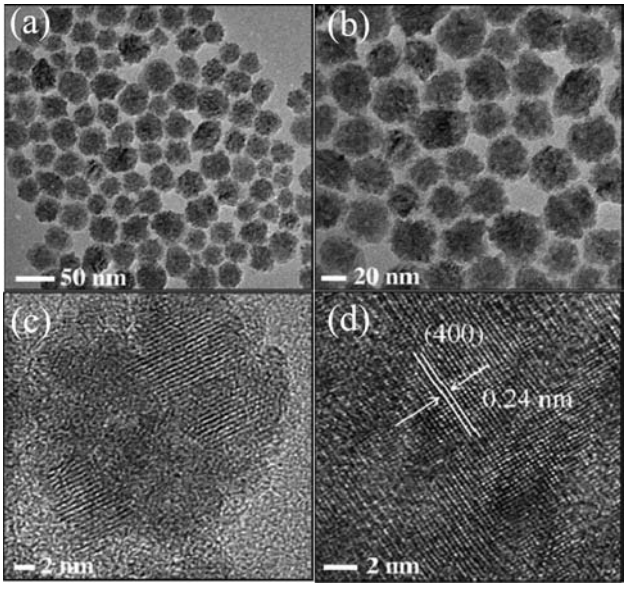

Figure 3. (a, b) TEM images of $CuCr_2S_4$ nanoclusters. (c, d) HRTEM images of an individual nanocluster.

nanoclusters with a size of 31 ± 2.5 nm composed of oblate-shaped smaller particles that were obtained using OLA as the solvent. The average size of the individual oblate particles was

dx.doi.org/10.1021/ja209575w | *J. Am. Chem.Soc.* 2011, 133, 20716–20719

difficult to determine, since the boundaries between the particles were not clearly observable in the TEM images. The measured distance between the lattice fringes from the HRTEM image in Figure 3d is 0.24 nm, corresponding to the (400) planes of cubic $CuCr_2S_4$.

The average elemental composition of samples suspended on Formvar-coated Ni grids was determined using energy-dispersive X-ray spectroscopy (EDX), which provided Cu/Cr/S ratios of 1:2:3.95 for the ODA-capped particles and 1:2:3.9 for the OLA-capped particles. These quantitative EDX values were obtained from different locations containing a large number of particles. The observed slight sulfur deficiency is likely due to the volatility of sulfur at the high reaction temperatures. To provide further confirmation of the distribution of Cu, Cr, and S within each particle, we performed STEM-EDX elemental mapping of individual nanocubes and nanoclusters. The mapping in Figure S4 shows the elemental homogeneity within a nanocluster.

The formation of nanocubes using ODA as a coordinating solvent appears to follow the classical atom-mediated crystallization process.[15] This type of growth phenomenon can be explained by the so-called Ostwald ripening process, in which the formation of larger particles is favored at the expense of smaller ones. Often, atoms, ions, or molecules serve as fundamental building blocks for this process. In this case, it is clear that the smallest units of the cubic spinel structure acts as intrinsic nuclei for the growth of bigger cubes. Such cube-shaped nanocrystal growth was previously observed for other spinels.[13c] In contrast, the observed nanoclusters obtained using OLA as a solvent may be the product of oriented-attachment crystal growth.[15,16] In this process, stable particles act as a mediating agent. For instance, this is observed in the smaller oblate-shaped primary units clubbed together to form a secondary mesocrystal. In this particle-mediated growth, random particles tend to self-organize with adjacent particles to share a common crystallographic orientation, which is followed by joining of these particles at a planar interface. A number of examples this type of oriented-attachment crystal growth, including for spinels, have been reported in the literature.[17]

ODA and OLA are structurally similar primary amines except for the shorter separation between ninth and 10th carbon atoms in OLA. It is interesting that this small difference in the two capping agents promotes totally different growth mechanisms for the formation of $CuCr_2S_4$. Restriction of the rotation because of the double bond at the 9-position in OLA perhaps enables the grains to rotate and attach together to attain a common orientation in order to reduce the surface energy. Flower-shaped nanoclusters of $CuCr_2Se_4$ were also observed when the synthesis was carried out using OLA and heptanoic acid.[13d] A detailed investigation of the influence of possible impurities in the OLA on the morphology and size of the nanoparticles is underway.

We analyzed the magnetic properties using a SQUID magnetometer to determine the blocking temperature and saturation magnetization of the nanocubes and nanoclusters. Figure 4 shows the variation of the magnetization as a function of temperature under field-cooled (FC) and zero-field-cooled (ZFC) conditions with applied magnetic fields of 50 and 100 Oe. The observed blocking temperatures (T_b) deduced from low-field (50 Oe) measurements for nanocubes and nanoclusters are ~290 and ~300 K, respectively. The measurements also showed a drop in the magnetization value to nearly zero at

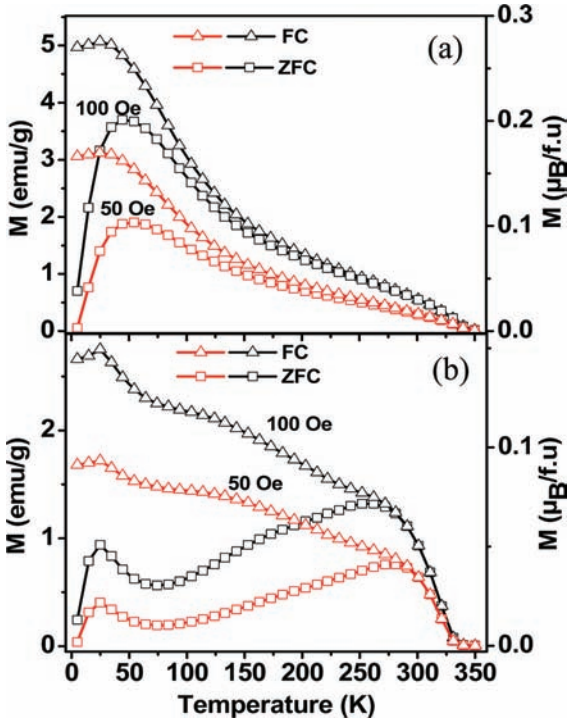

Figure 4. Magnetization (M) as a function of temperature for field-cooled (FC) and zero-field-cooled (ZFC) measurements at 100 and 50 Oe for (a) nanocubes and (b) nanoclusters of $CuCr_2S_4$.

temperatures between 340 and 345 K for both samples (Figure 4). This can be ascribed to their T_C's, which are somewhat lower than the bulk value of 377 K.[7]

The magnetizations of the two samples were measured as functions of external magnetic field to evaluate the saturation magnetization at 5 and 300 K (Figure 5). Both types of nanoparticles exhibit superparamagnetic (SP) behavior near room temperature (Figure 5a), whereas ferromagnetic behavior with relatively lower coercivity values of ~350 Oe (nanocubes) and ~750 Oe (nanoclusters) was observed at 5 K (Figure 5b inset). Interestingly, neither loop saturates even at a magnetic field of 5 T. The highest magnetization value obtained at 5 K for nanocubes was 30 emu/g (1.63 μ_B/f.u.), and that for nanoclusters was estimated to be 33 emu/g (1.79 μ_B/f.u.). These values are lower than the reported bulk value of 86 emu/g,[14] but part of the reason could be due to the unaccounted weight of the capping layer. Nevertheless, the magnetization values are much higher than the reported value for nanoparticles synthesized by ball milling (18 emu/g).[14]

The observed magnetization behavior of these particles may be associated with size and shape anisotropy or spin-glass state at low temperatures. It is well-known that defects created by vacancies at cation and anion sites, as well as the broken symmetry at the particle surface, can significantly reduce the effective number of spins, leading to a decrease in the net magnetization and nonsaturation of the loops due to possible antiferromagnetic coupling.[18] In the Figure S5 inset, the enlarged image of the boxed area in the HRTEM image of a nanocube does show evidence of defects on the surface. We also estimated the lateral size of the SP particles by fitting the magnetization value measured at 300 K with the Langevin function (Figure S6). Langevin fits gave average particle sizes of 15 nm for nanocubes and 21 nm for nanoclusters. While the estimated size of the nanocubes is close to that observed by

dx.doi.org/10.1021/ja209575w | J. Am. Chem.Soc. 2011, 133, 20716–20719

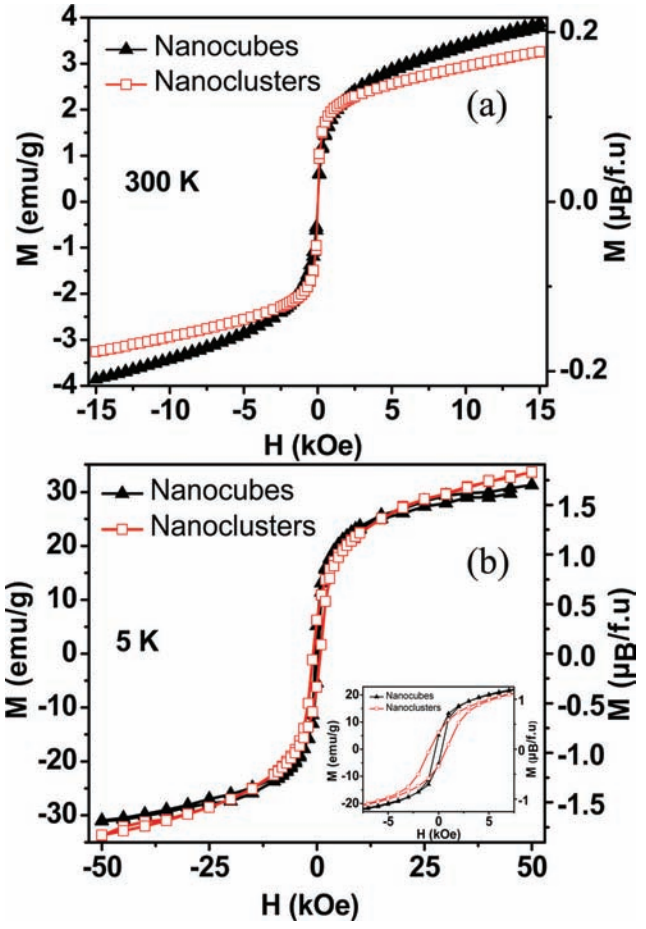

Figure 5. Magnetization (M) as a function of field (H) for $CuCr_2S_4$ nanocubes and nanoclusters at (a) 300 K and (b) 5 K. The inset in (b) displays an enlarged portion showing the coercivities of the two samples.

TEM, there is a deviation in the estimated size for the nanoclusters. This deviation is likely due to the particles being closer to the SP limit.[13c]

In summary, we have demonstrated a novel approach for the colloidal synthesis of $CuCr_2S_4$ nanocrystals and nanoclusters. The method involves hot injection of 1-dodecanethiol into a boiling coordinating solvent containing metal salts. The reaction using octadecylamine results in the formation of cube-shaped nanocrystals, whereas oleylamine yields flower-shaped nanoclusters. While the particles exhibit superparamagnetic behavior close to room temperature, they are ferromagnetic at lower temperatures, with magnetization values of 30 emu/g for the nanocubes and 33 emu/g for the nanoclusters at 5 K. The synthesis of other chalcospinels of general formula MCr_2X_4 (M = Cd, Pb, Sn; X = S, Se, Te) following this synthetic protocol is under investigation, and the results will be reported elsewhere.

■ ASSOCIATED CONTENT

Supporting Information

Reaction scheme; XRD, TEM, SEM, and EDX images; STEM-EDX elemental mapping; Langevin fit; and experimental details. This material is available free of charge via the Internet at http://pubs.acs.org.

■ AUTHOR INFORMATION

Corresponding Author

agupta@mint.ua.edu

■ ACKNOWLEDGMENTS

This work was supported by the National Science Foundation under Grant CHE-1012850. The authors are grateful to Dr. Prahallad Padhan for helpful suggestions regarding the magnetic measurements.

■ REFERENCES

(1) (a) Batlle, X.; Labarta, A. *J. Phys. D: Appl. Phys.* **2002**, *35*, R15. (b) Frenkel, J.; Dorfman, J. *Nature* **1930**, *126*, 274. (c) Bean, C. P.; Livingston, J. D. *J. Appl. Phys.* **1959**, *30*, 1205. (d) Zarur, A. J.; Ying, J. Y. *Nature* **2000**, *403*, 65.

(2) (a) Berkovsky, B. M.; Medvedev, V. F.; Krokov, M. S. *Magnetic Fluids: Engineering Applications*; Oxford University Press: Oxford, U.K., 1993. (b) Ziolo, R. F.; Giannelis, E. P.; Weinstein, M. P.; O'Horo, B. N.; Ganguly, M. V.; Russel, M. W.; Huffman, D. R. *Science* **1992**, *257*, 219.

(3) Hyeon, T. *Chem. Commun.* **2003**, 927.

(4) (a) Murray, C. B.; Sun, S.; Gaschler, W.; Doyle, H.; Betley, T. A.; Kagan, C. R. *IBM J. Res. Dev.* **2001**, *45*, 47. (b) Murray, C. B.; Sun, S.; Doyle, H.; Betley, T. A. *MRS Bull.* **2001**, 985. (c) Wang, Z. L.; Dai, Z.; Sun, S. *Adv. Mater.* **2000**, *12*, 1944. (d) Rockenberger, J.; Scher, E. C.; Alivisatos, A. P. *J. Am. Chem. Soc.* **1999**, *121*, 11595. (e) Hyeon, T.; Lee, S. S.; Park, J.; Chung, Y.; Na, H. B. *J. Am. Chem. Soc.* **2001**, *123*, 12798. (f) Shen, S.; Zeng, H. *J. Am. Chem. Soc.* **2002**, *124*, 8204.

(5) Fedorov, V. A.; Kesler, Y. A.; Zhukov, E. G. *Inorg. Mater.* **2003**, *39*, S68.

(6) Lotgering, F. K. *Solid State Commun.* **1964**, *2*, 55.

(7) (a) Goodenough, J. B. *Solid State Commun.* **1967**, *5*, 577. (b) Baltzer, P. K.; Lehmann, H. W.; Robbins, M. *Phys. Rev. Lett.* **1965**, *15*, 493.

(8) Van Stapele, R. P. In *Ferromagnetic Materials*; Wohlfarth, E. P., Ed.; North-Holland: Amsterdam, 1982; Vol. 3, p 8.

(9) Antonov, V. N.; Antropov, V. P.; Harmon, B. N.; Yaresko, A. N.; Perlov, A. Ya. *Phys. Rev. B* **1999**, *59*, 14552.

(10) Saha-Dasgupta, T.; De Raychaudhury, M.; Sarma, D. D. *Phys. Rev. B* **2007**, *76*, No. 054441.

(11) Wang, Y.-H. A.; Gupta, A.; Chshiev, M.; Butler, W. H. *Appl. Phys. Lett.* **2009**, *94*, No. 062515.

(12) Ramirez, A. P.; Cava, R. J.; Krajewski, J. *Nature* **1997**, *386*, 156.

(13) (a) Ramesha, K.; Seshadri, R. *Solid State Sci.* **2004**, *6*, 841. (b) Kim, D.; Gedanken, A.; Tver'yanovich, Y. S.; Lee, D. W.; Kim, B. K. *Mater. Lett.* **2006**, *60*, 2807. (c) Wang, Y. H. A.; Bao, N.; Shen, L.; Padhan, P.; Gupta, A. *J. Am. Chem. Soc.* **2007**, *129*, 12408. (d) Lin, C. R.; Yeh, C. L.; Lu, S. Z.; Lyubutin, I. S.; Wang, S. C.; Suzdalev, I. P. *Nanotechnology* **2010**, *21*, No. 235603.

(14) Muroi, M.; Street, R.; McCormick, P. G. *Phys. Rev. B* **2001**, *63*, No. 052412.

(15) Fang, J.; Ding, B.; Gleiter, H. *Chem. Soc. Rev.* **2011**, *40*, 5347.

(16) (a) Fang, J. X.; Du, S. Y.; Li, Z. Y.; Lebedkin, S.; Kruk, R.; Hahn, H. *Nano Lett.* **2010**, *10*, 5006. (b) Lim, B.; Lu, X.; Jiang, M.; Camargo, P. H. C.; Cho, E. C.; Lee, E. P.; Xia, Y. *Nano. Lett.* **2008**, *8*, 4043.

(17) (a) Cho, K. S.; Talapin, D. V.; Gaschler, W.; Murray, C. B. *J. Am. Chem. Soc.* **2005**, *127*, 7140. (b) Bao, N.; Shen, L.; Wang, Y.-H. A.; Ma, J.; Mazumdar, D.; Gupta, A. *J. Am. Chem. Soc.* **2009**, *131*, 12900.

(18) Luigjes, B.; Woudenberg, S. M. C.; Groot, R. D.; Meeldijk, J. D.; Galvis, H. M. T.; Jong, K. P. D.; Philipse, A. P.; Erne, B. H. *J. Phys. Chem. C* **2011**, *115*, 14598.